J. Micromech. Microeng. **20** (2010) 035028 (7pp) doi:10.1088/0960-1317/20/3/035028

Design and fabrication of a single membrane push-pull SPDT RF MEMS switch operated by electromagnetic actuation and electrostatic hold

Il-Joo Cho and Euisik Yoon

Department of Electrical Engineering and Computer Science, University of Michigan, 1301 Beal Ave, Ann Arbor, MI 48109, USA

E-mail: ijcho@umich.edu

Received 25 August 2009, in final form 13 January 2010
Published 2 March 2010
Online at stacks.iop.org/JMM/20/035028

Abstract

In this paper, we report a new push-pull-type SPDT (single pole double throw) switch actuated by the combination of electromagnetic and electrostatic forces for low power and low voltage operation. The switch is initially actuated by large electromagnetic force to change its state and is held to maintain its state by applying electrostatic force to reduce static power consumption. The electromagnetic force can be easily generated at low voltage. The maximum actuation voltage is below 4.3 V and the required energy is 15.4 μJ per switching. It achieves signal isolation of -54 dB and insertion loss of -0.16 dB at 2 GHz, respectively. For 20 GHz operation, isolation and insertion loss were measured as -36 dB and -0.52 dB, respectively. The proposed SPDT switch combines two switching elements in a single structure, simplifying the overall structure and control signals and eliminating mismatches between the two switching elements. The dimension of the switch has been optimized using FEM simulation and analytical calculations. We have successfully carried out a lifetime test over more than 166 million cycles with the maximum actuation voltage below 4.3 V.

(Some figures in this article are in colour only in the electronic version)

1. Introduction

RF switch is an essential component to handle RF signals in wireless communication systems, which has made an explosive growth in emerging consumer markets as well as military applications. Especially, SPDT (single pole double throw) switch is a switching element widely used in the applications of wireless communication systems and measurement equipment where multiple inputs of high frequency signals should be connected to any arbitrary outputs. It consists of a single input port and double output ports and should always connect the input port to one of the two output ports. SPDT switch designs have traditionally evolved from solid-state devices such as FETs or PIN diodes, which require large power consumption and degrade their performance at high frequencies [5, 6].

To solve these problems, several high performance SPDT switches have been introduced using MEMS technologies [1–3]. All the previously reported MEMS SPDT switches have been implemented using two identical switching structures actuated by electrostatic force [8–15]. These topologies have employed two separate structures; therefore, they require two conjugate actuation signals which must be synchronized to guarantee a connection path between one of the input and output ports. Therefore, any mismatches between switching structures may produce asymmetrical switching characteristics when observed in the output port. Although the RF MEMS switches actuated by electrostatic force offer extremely low power consumption and relatively simple implementation, there still remain two main challenging issues: lowering the actuation voltage and increasing mechanical stability. The high actuation voltage degrades lifetime and induces malfunction by a charge trapping problem in the dielectric

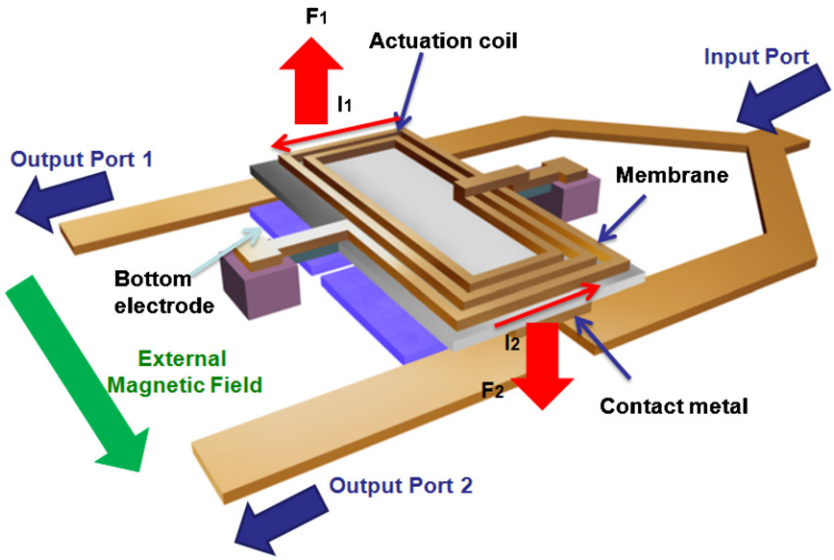

Figure 1. Schematic diagram of the proposed push-pull SPDT RF MEMS switch.

layer [16]. In order to lower the actuation voltage, new switch concepts using meander spring suspensions and push-pull structures have been investigated [17, 18]. However, these approaches showed poor mechanical properties because the spring constant of the switch was designed so low to lower the actuation force. This small spring constant for low actuation voltage makes it difficult for the switches to be mechanically robust and to provide high isolation due to the restriction imposed on the maximum initial gap. In addition, high actuation voltage makes it difficult to be integrated with other devices and controlled by standard CMOS circuitry.

In this work, we first propose a new push-pull-type SPDT switch formed in a single switching structure actuated by the combination of electromagnetic and electrostatic forces with an external magnetic field. The proposed switch structure is composed of only one symmetric membrane and it rotates along a torsion bar. Therefore, one of the output ports is always connected to the input port as for conventional SPDT switches. This single structure not only simplifies the design and control signals but also eliminates performance mismatch between two switching paths. The proposed switch utilizes the combined actuation mechanism of electromagnetic actuation and electrostatic holding which was reported in the application of SPST switches by our group [19]. When the proposed switch changes its state, it uses electromagnetic force and it maintains its state by electrostatic force. Power is consumed only during the electromagnetic actuation for a very short amount of time, and the switch will be in electrostatic holding mode which consumes negligible power during the remaining period. Therefore, the switch can operate at low voltage and low power consumption. Also, the large electromagnetic force generated using an external magnetic field [19–21] enables the SPDT switch to achieve high isolation at off-state, immunity to vibration and high power handling capability. The proposed switch concept is suitable for both series and shunt SPDT switch implementations. However, in this paper we will only discuss and focus on a metal-to-metal contact series-type SPDT switch configuration.

2. Structure and operation

The proposed SPDT switch using a push-pull-type MEMS structure is shown in figure 1. The switching structure is implemented in a suspended single dielectric membrane integrated with actuation coils for electromagnetic actuation. For electrostatic holding, we implemented the bottom electrodes to apply the electrostatic potential between the coils and the electrode. The CPW lines will be connected by the contact metals located at each end of the membrane when it is actuated by electromagnetic force. The membrane structure is supported by two torsion bars which are composed of dielectric films, and thick coils to enhance the mechanical stability of the structure. Also, the coils on the membrane are connected to the bottom metal layer to supply the actuation current. The structure is symmetrical and the membrane rotates along the torsion bars. Therefore, one of the output ports is always connected to the input port except for the initial condition right after fabrication. The symmetrical push-pull structure of the proposed SPDT switch can reduce any mismatch in the characteristics between the two outputs and simplify control signals.

Figure 2 shows the timing diagram of control signals actuated by the combination of electromagnetic and electrostatic forces. Initially, two contact metals are detached from the signal lines by an initial gap. When the actuation current is applied to the coil in a counterclockwise direction as shown in figure 1, the membrane rotates along the torsion bars. Accordingly, the contact metal above the output port 2 is actuated downward and makes a connection to the underlying CPW signal lines by electromagnetic force F2. The other contact metal in the opposite side moves upward and the distance between the contact metal and the signal line increases. This push-pull operation improves the isolation at off-state. After one of the contact metals actuates downward, the actuation current is turned off and only the electrostatic force between the coils and the bottom electrode holds the membrane and maintains its ‘on’ state without static power

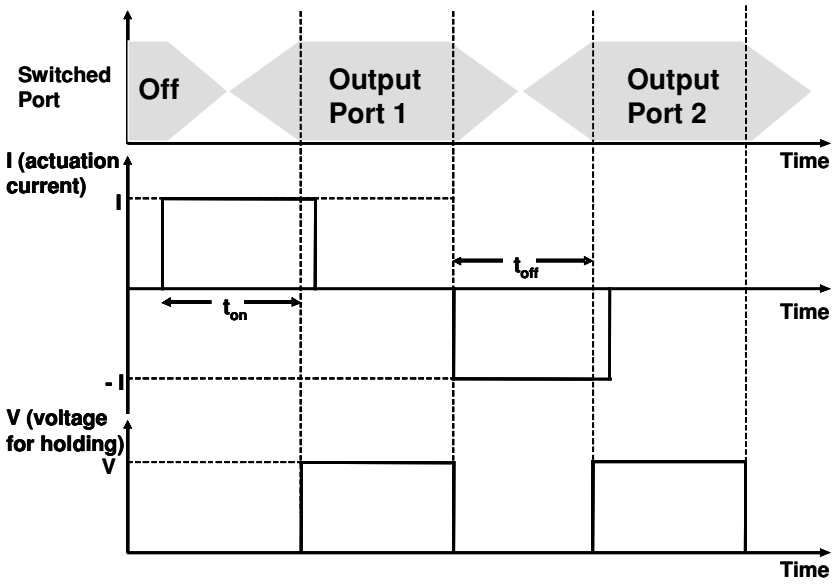

Figure 2. Timing diagram of control signals for switching operation.

consumption. In order to switch the input port to the output port 1, the actuation current should be applied in a clockwise direction and the contact metal above the output port 1 actuates downward and the contact metal above the output port 2 moves upward by electromagnetic force as well as mechanical restoring force. This large restoring force enables the contact metal to be easily detached from the bottom metal while applying signal currents, so-called hot switching. This results in less risk of stiction between the metal contact and the signal lines. The stiction is a serious problem to make the switch closed permanently due to micro-welding effect which typically happens at a signal power greater than 20 dBm [22, 23]. The push-pull magnetic actuation of the proposed SPDT switch improves power-handling capability.

The combination of two different actuation mechanisms, electromagnetic and electrostatic forces, provides a few other merits. The electromagnetic actuation force is constant regardless of an initial gap of the membrane from the bottom plane, while the electrostatic force is inversely proportional to the square of the gap. This allows us to make an initial gap large enough to realize high signal isolation which is difficult to achieve in electrostatic actuation. Also, we can attain high power handling capability from large restoring force and good immunity to vibration from high spring constant structure. In addition, operation voltages can be maintained below 5 V because the electrostatic force is only applied during the holding stage when a small gap is already formed between the bottom electrode and the coils. Electromagnetic force is only required during the short period of time for switching its states. Therefore, the proposed SPDT switch can operate at low voltage as well as at low power consumption.

3. Design and simulations

To design and optimize the structures of the proposed SPDT RF MEMS switch, analytical calculations and FEM simulations using Coventoware were conducted. The proposed switch is actuated by electromagnetic force and the force from an external magnetic field is expressed as

$$F_{\text{Lorentz}} = 2I \oint \mathrm{d}l \times B(l) \tag{1}$$

where I is the actuation current, B is the magnetic field from external permanent magnets and l is the summation of coil lengths perpendicular to the direction of the magnetic field. To acquire maximum electromagnetic force, the coil length should be optimized at the given current and magnetic field. Also, spring constant should be optimized. In this design, FEM simulation is used to predict the actuation current as shown in figure 3(*a*). The simulated spring constant is 3.2 N m^{-1} and the minimum current required for actuation is 50 mA for 10 μm displacement when the number of turns in the coil is five ($N = 5$). Electrostatic holding voltage can be estimated from the electrostatic force

$$F_{\text{electrostatic}} = \frac{\varepsilon_r \varepsilon_o A_{\text{eff}} V_{\text{Pull-out}}^2}{2t_{\text{SiN}}^2}, \tag{2}$$

where A_{eff} is the effective area of the coil to generate electrostatic force and t_{SiN} is the dielectric thickness between the bottom metal and the coil. In this equation, V_{holding} can be determined when the electrostatic force is equal to the restoring force when it is actuated. Therefore, the minimum holding voltage can be found:

$$V_{\text{holding}} = \sqrt{\frac{2kgt_{\text{SiN}}^2}{\varepsilon_r \varepsilon_0 A_{\text{eff}}}}, \tag{3}$$

where k is the spring constant of the structure and g is the initial gap between the electrodes. In order to have a small holding voltage, we have to maximize the effective area and minimize the dielectric thickness. In the proposed design, A_{eff} is 200 μm $\times$ 200 μm and the dielectric thickness is 0.2 μm. By using equation (3), the required holding voltage is estimated to be less than 1.5 V with an initial gap of 10 μm. The mechanical

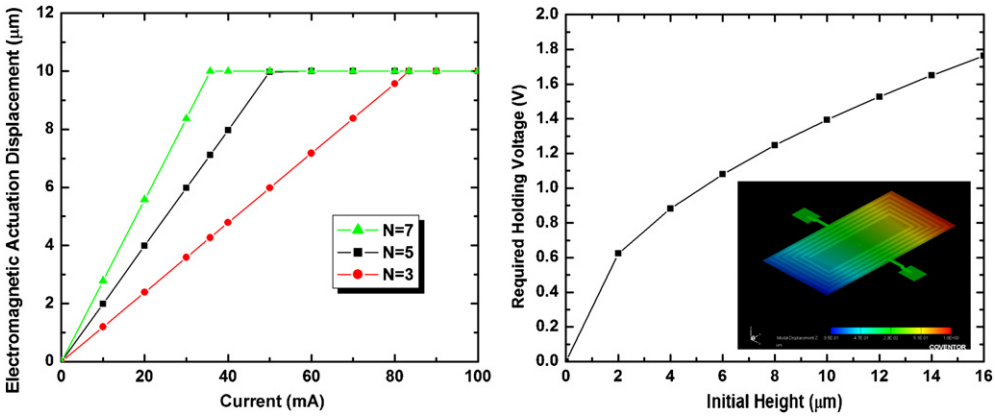

(*a*) (*b*)

Figure 3. Simulation and analytical calculation of (*a*) electromagnetic actuation displacement as a function of the actuation current where *N* is the number of turns in the coil and (*b*) required holding voltage for various initial heights.

Table 1. Dimensions of the proposed SPDT switch.

		Dimension			Dimension
Membrane	Width	500 μm	Torsion bar	Width	20 μm
	Length	1000 μm		Length	100 μm
	Thickness	3.6 μm		Thickness	3.6 μm
Coil	Width	15 μm	CPW line	Thickness	0.5 μm
	Spacing	15 μm		Width	65 μm
	Thickness	3 μm		Length before Tee junction	300 μm
				Length after Tee junction	1400 μm
Contact metal thickness		0.5 μm			
Bottom electrode		400 μm $\times$ 250 μm	Initial gap		10 μm
Electromagnetic force		46.2 μN	Spring constant		3.3 N m^{-1}

resonant frequency is simulated as 3.95 kHz; this means that the switch response time can be in the order of a millisecond. Table 1 summarize the detailed dimensions of the proposed SPDT switch.

4. Fabrication

Fabrication processes of the proposed MEMS SPDT switch can be found in the previously reported RF MEMS switch by the same group [19]. It is made on the glass wafer to reduce substrate loss of RF signals. By using polyimide film as a sacrificial layer, the SPDT switch membrane is fabricated using dielectric layers and electroplated gold layers as shown in figure 4. The membrane is composed of three layers: the first nitride layer, an electroplated gold layer and the second nitride layer. In this structure, the first nitride layer thickness (200 nm) is minimized to obtain a low holding voltage because the total nitride film thickness affects the electrostatic force during the holding period. After patterning the first nitride layer, Cr/Au is deposited for a seed metal and gold (about 3 μm) is electroplated. Next, the second nitride layer (600 nm) is deposited and patterned. This second nitride layer plays an important role in releasing the residual stress of the membrane as well as enhancing the mechanical stability. This sandwich structure, which is composed of a first nitride layer, a Au layer and a second nitride layer, compensates the stress and a stress-free membrane can be obtained. The total thickness of the membrane is about 3.8 μm, and this thick structure can enhance the mechanical stability. Next, another Cr/Au layer (20 nm/500 nm) is patterned using liftoff for interconnection metal. This bridge metal layer electrically connects the coils to external pads through the torsion bars. The electrical isolation between the bridge metal and the electroplated gold coil is achieved by dielectric isolation using the second nitride layer.

The fabricated MEMS SPDT switch is shown in figure 4. The figures show that the stress of the membrane has been fully compensated and the membrane is stress free. There are three control signal lines for actuation of the fabricated SPDT switch: one actuation signal and two holding signals. A single input port and two output ports for SPDT configuration are implemented in CPW signal lines. The input CPW signal line is branched off to two signal lines and connected with two output ports. In the middle of each signal line, there is a cut-off region below contact metals to perform a switch. The distance between the bottom electrode and the membrane is about 12.7 μm. This is about four times larger than that of the previously reported MEMS switches [1, 17] and provides high signal isolation in off-state. Also, the area of gold coils has

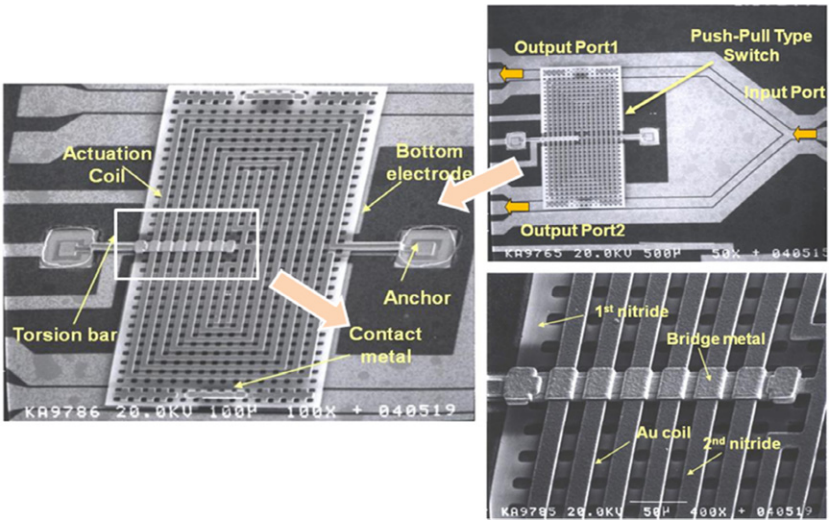

Figure 4. SEM pictures of the fabricated SPDT RF MEMS switch.

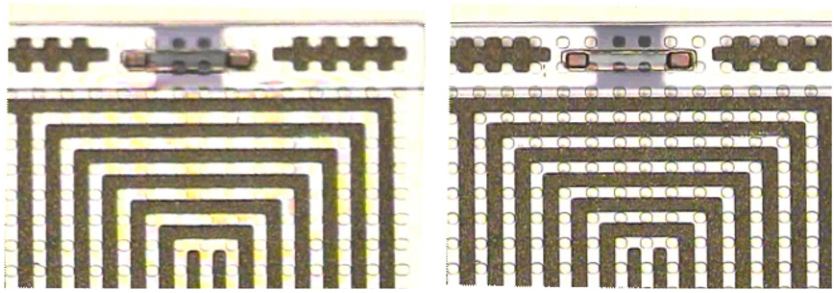

(*a*) (*b*)

Figure 5. Microscope images of the actuated SPDT RF MEMS switch: (*a*) off-state when the contact metal is detached from the CPW line and (*b*) on-state when the contact metal is connected to the CPW line.

been maximized to reduce the holding voltage by increasing the effective area for electrostatic force.

5. Measurement results

5.1. Mechanical characteristics

Mechanical characteristics of the fabricated switch have been characterized during the operation of the switch using Polytec's LDV (laser Doppler vibrometer). Figure 5(*a*) shows a gap between CPW lines and the membrane in off-state. The membrane is blurred while the CPW line is clearly in focus. Figure 6(*b*) shows the on-state of the switch where both the membrane and the CPW lines are in focus. You can clearly see the etch holes in the membrane. The displacement and resonance frequency of the actuated membrane are measured as shown in figure 6. The displacement is linear as a function of applied actuation current and the actuation force remains constant during the displacement. This can significantly reduce any possible mechanical damage to the contact metals at the time of switching. In the case of electrostatic actuation, the force is inversely proportional to the gap between the two electrodes. Therefore, the actuation is accelerated as the contact metal approaches to make electrical connection, resulting in a serious reliability problem due to the damage

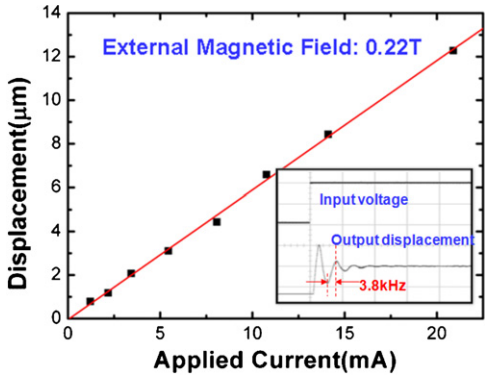

Figure 6. Measured displacement of the fabricated SPDT switch as a function of the applied actuation current.

on the metals. Resonant frequency has been measured as 3.8 kHz.

With an applied current of 23 mA, we can successfully actuate the switch to on-state. The holding voltage for maintaining its state has been measured below 4.3 V. The switching time and the power consumption have been estimated from dynamic response of the fabricated switch, respectively. The switching time is estimated to be 132 μs for the transition from on- to off-state and 447 μs for the transition

Table 2. Comparison table with previous SPDT RF MEMS switches.

	Number of membranes	Actuation mechanism	Type	Actuation voltage	Insertion loss	Isolation	Frequency
Michigan [1]	2	Electrostatic	Shunt	9 V	−0.69 dB	−40 dB	20 GHz
LAAS-CNRS [2]	2	Electrostatic	Shunt	35 V	−0.6 dB	−21 dB	30 GHz
IMST [3]	2	Electrostatic	Series	4 V	−0.47 dB	−28 dB	30 GHz
SNU [4]	2	Electrostatic	Series	35 V	−0.45 dB	−22 dB	47 GHz
Nanyang [7]	2	Electrostatic	Series	23 V	−0.75 dB	−19 dB	5 GHz
This work	1	Electro-magnetic	Series	4.3 V	−0.52 dB to −2.05 dB	−36 dB	20 GHz

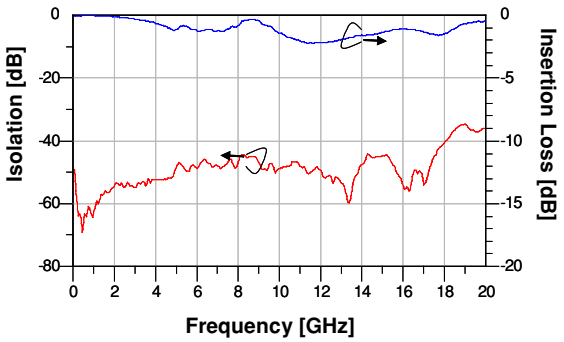

Figure 7. Measured RF characteristics of the fabricated SPDT switch: isolation for off-state and insertion loss for on-state.

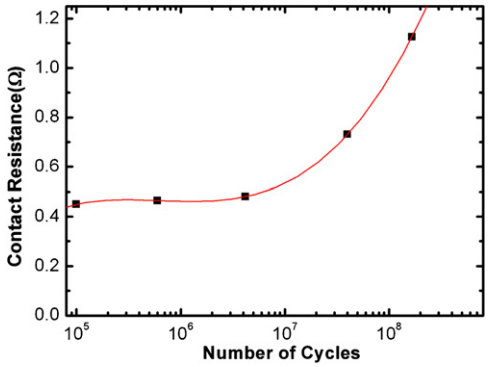

Figure 8. Measured contact resistance as a function of a number of switching cycles.

from off- to on-state. The required energy for switching is estimated to be 15.4 μJ. This is an extremely small value because the switch consumes power only during the transition of its states.

5.2. *RF characteristics*

RF performances of the fabricated SPDT MEMS switch have been characterized using an Agilent 8510C network analyzer. External electrical control signals are applied on the fabricated switch for actuation, and S-parameters are measured and extracted from the input and output ports. Figure 7 shows the measured RF characteristics of the fabricated SPDT MEMS switch. The isolation represents the performance of the switch for off-state. The isolation value has been measured from S21 parameters when the contact metal is detached from the bottom signal lines. The measured isolation is −54 dB at 2 GHz and −36 dB at 20 GHz. This high isolation can be achieved due to a large initial gap. During off-state, the main source of signal coupling from the input to the output port is from the overlap capacitance between cut-off signal lines and contact metal. In the fabricated RF MEMS switch, this coupling capacitance is measured less than 1.2 fF because of the large initial gap.

The insertion loss of the switch has been characterized by using S21 parameters during on-state. The measured insertion loss is −0.16 dB at 2 GHz and −0.52 dB at 20 GHz. These numbers are comparable to the previous RF MEMS switches. However, the measured insertion loss shows a maximum value of −2.05 dB at 12 GHz. Figure 7 shows a few local maximum points of insertion loss at approximately 6 GHz, 12 GHz and 18 GHz, and these local maximum values are thought to be the unwanted resonance effects in the device. There are some parasitic capacitances and inductances in the device, and the combinations of these components make resonances with low Q-factor and the S21 parameters fluctuate at these frequencies. For example, as shown in figure 5, actuation coils and signal lines make some parasitic inductances and capacitances and they can make resonance at certain frequencies. Also, there should be other parasitic components and they make the S21 parameters fluctuate. To minimize these effects, the distance between CPW lines and actuation coils should be increased and other parasitic components should be eliminated.

Table 2 summarizes the measured characteristics of the fabricated switch compared with those of other previously reported SPDT RF MEMS switches. The fabricated switch shows comparable performances in insertion loss, isolation and actuation voltage while it is implemented in a simple structure of a single membrane.

5.3. *Reliability test*

In order to estimate the lifetime of the fabricated MEMS SPDT switch, a reliability test has been performed. The initial contact resistance was 0.42 Ω and it has been maintained until 4.2 million switching cycles. However, it starts to increase slightly up to 1.13 Ω after 166 million cycles. This degradation of contact resistance is mainly due to the wear of contact metals by continuously hitting two metal contacts. We have not observed any noticeable change in the operation voltage and actuation current within a measurement error range even after 166 million cycles as shown in figure 8. This shows that the fabricated SPDT switch can operate mechanically robust and electrically stable up to 100 million cycles.

6. Conclusions

We have proposed and implemented a new low voltage and low power MEMS SPDT switch in a single push-pull structure. The initial design has been optimized using FEM simulation and analytical calculations. The proposed MEMS SPDT switch has been implemented in a symmetrical single membrane to eliminate any possible mismatches between output ports. The fabricated push-pull RF MEMS switch is actuated by the combination of electromagnetic and electrostatic forces at low actuation voltage and low power consumption. The fabricated SPDT switch can be actuated below 4.3 V and consume energy below 15.4.μJ per switching. The isolation has been measured as -54 dB at 2 GHz and -36 dB at 20 GHz. The insertion loss has been measured as -1.23 dB at 6 GHz and -0.52 dB at 20 GHz. To reduce the insertion loss further in the entire operation frequency range, CPW lines should be optimized to alleviate the short stub effect. The fabricated switch has successfully demonstrated stable operation after 166 million cycles of actuation. The low voltage and low power features of the fabricated switch may allow it to be easily integrated with other RF components and extend its possibility to CMOS integration as a viable SoC solution for future wireless communication products.

References

[1] Pacheco S, Peroulis D and Katehi L 2001 MEMS single-pole double-throw (SPDT) X and K-band switching circuits *IEEE MTT-S Int. Microwave Symposium Digest* vol 1 pp 321–4

[2] Dubuc D, Rabbia L, Grenier K, Pons P, Vendier O, Graffeuil J and Plana R 2003 Original MEMS-based single pole double throw topology for millimeter wave space communications *European Microwave Conf.* vol 3 pp 979–82

[3] Schauwecker B, Strohm K, Mack T, Simon W and Luy J 2003 Single-pole-double-throw switch based on toggle switch *Electron. Lett.* **39** 668–70

[4] Park J, Lee S, Kim J, Kwon Y and Kim Y 2003 A 35–60 GHz single-pole double-throw (SPDT) switching circuit using direct contact MEMS switches and double resonance technique *12th Int. Conf. on TRANSDUCERS, Solid-State Sensors, Actuators and Microsystems* pp 1796–9

[5] Kobayashi K, Tran L, Oki A and Streit D 1995 A 50 MHz–30 GHz broadband co-planar waveguide SPDT PIN diode switch with 45-dB isolation *IEEE Microw. Guid. Wave Lett.* **5** 56–8

[6] Teeter D, Wohlert R, Cole B, Jackson G, Tong E, Saledas P, Adlerstein M, Schindler M, Shanfield S and Div R 1994 Ka-band GaAs HBT PIN diode switches and phase shifters *IEEE MTT-S Int. Microwave Symposium Digest* pp 451–4

[7] Tang M, Liu A, Agarwal A, Liu Z and Lu C 2005 A single-pole double-throw (SPDT) circuit using lateral metal-contact micromachined switches *Sensors Actuators* A **121** 187–96

[8] Peroulis D, Pacheco S, Sarabandi K and Katehi P 2000 MEMS devices for high isolation switching and tunable filtering *IEEE MTT-S Int. Microwave Symposium Digest.* pp 1217–20

[9] Larson L, Hackett R and Lohr R 1991 Microactuators for GaAs-based microwave integrated circuits *TRANSDUCERS'91. Int. Conf.* pp 743–6

[10] Goldsmith C, Randall J, Eshelman S, Lin T, Denniston D, Chen S, Norvell B, Inc T and Dallas T 1996 Characteristics of micromachined switches at microwave frequencies *IEEE MTT-S Int. Microwave Symposium Digest.* pp 1141–4

[11] Goldsmith C, Yao Z, Eshelman S and Denniston D 1998 Performance of low-loss RF MEMS capacitive switches *IEEE Microw. Guid. Wave Lett.* **8** 269–71

[12] Yao Z, Chen S, Eshelman S, Denniston D and Goldsmith C 1999 Micromachined low-loss microwave switches *J. Microelectromech. Syst.* **8** 129–34

[13] Muldavin J and Rebeiz G 2000 High-isolation CPW MEMS shunt switches: 1. Modeling *IEEE Trans. Microw. Theory Tech.* **48** 1045–52

[14] Shen S and Feng M 1999 Low actuation voltage RF MEMS switches with signal frequencies from 0.25 GHz to 40 GHz *Proc. Int. Electron Devices Meeting* pp 689–92

[15] Park J, Kim G, Chung K and Bu J 2000 Electroplated RF MEMS capacitive switches *13th Annual Int. Conf. on Micro Electro Mechanical Systems, 2000* pp 639–44

[16] Rebeiz G and Muldavin J 2001 RF MEMS switches and switch circuits *IEEE Microw. Mag.* **2** 59–71

[17] Hah D and Hong S 2000 A low-voltage actuated micromachined microwave switch using torsion springs and leverage *IEEE Trans. Microw. Theory Tech.* **48** 2540–45

[18] Pacheco S, Katehi L and Nguyen C 2000 Design of low actuation voltage RF MEMS switch *IEEE MTT-S Int. Microwave Symposium Digest* pp 156–8

[19] Cho I, Song T, Baek S and Yoon E 2005 A low-voltage and low-power RF MEMS series and shunt switches actuated by combination of electromagnetic and electrostatic forces *IEEE Trans. Microw. Theory Tech.* **53** 2450–7

[20] Cho I and Yoon E 2009 A low-voltage three-axis electromagnetically actuated micromirror for fine alignment among optical devices *J. Micromech. Microeng.* **19** 085007

[21] Im M, Cho I, Yun K and Yoon E 2007 Electromagnetic actuation and microchannel engineering of a polymer micropen array integrated with microchannels and sample resevoirs for biological assay patterning *Appl. Phys. Lett.* **91** 124101

[22] Oberhammer J and Stemme G 2004 Low-voltage high-isolation DC-to-RF MEMS switch based on an S-shaped film actuator *IEEE Trans. Electron Devices* **51** 149–55

[23] Hyman D and Mehregany M 1999 Contact physics of gold microcontacts for MEMS switches *IEEE Trans. Compon. Packag. Technol.* **22** 357–64